Supplementary Information

High adsorption of ammonia in a titanium–based metal-organic framework

Xiangdi Zeng,[a] Jiangnan Li,[a,b] Meng He,[a] Wanpeng Lu,[a] Danielle Crawshaw,[a] Lixia Guo,[a,b] Yujie Ma,[a] Meredydd Kippax-Jones,[a,c] Yongqiang Cheng,[d] Pascal Manuel,[e] Svemir Rudić,[e] Mark D. Frogley,[c] Martin Schröder[a*] and Sihai Yang[a,b*]

a. Department of Chemistry, University of Manchester, Manchester, M13 9PL, UK.
MSchroder@manchester.ac.uk; Sihai.Yang@manchester.ac.uk

b. College of Chemistry and Molecular Engineering, Beijing National Laboratory for Molecular Sciences, Peking University, Beijing, 100871, China
Sihai.Yang@pku.edu.cn

c. Diamond Light Source, Harwell Science Campus, Oxfordshire, OX11 0DE, UK.

d. Neutron Scattering Division, Neutron Sciences Directorate, Oak Ridge National Laboratory, Oak Ridge, TN 37831, USA

e. ISIS Neutron and Muon Facility, Rutherford Appleton Laboratory, Didcot, OX11 0QX, UK.

Content

Experimental Section

Synthesis of {Ti_8AF} cluster

The {Ti_8AF} cluster was synthesised according to the published method[1]. To a 250 mL round-bottomed flask, formic acid (100 mL), acetic anhydride (100 mL), were added with stirring at room temperature. $Ti(iPrO)_4$ (20 mL) was then slowly added to the solution. The mixture was refluxed at 120°C for 12 h, and after cooling to room temperature, the white product was collected by filtration or centrifugation and washed in boiling acetone.

Synthesis of MFM-300(Ti)

{Ti_8AF} (220 mg, 0.16mmol) and H_4bptc (330 mg, 1.0 mmol) were placed into a 23 mL Teflon reactor followed by the addition of acetic anhydride (5 mL) and acetic acid (5 mL). After stirring for 10 min, MeOH (0.5 mL) was added, and the mixture stirred at room temperature for a further 10 mins. The reaction was then heated in an oven at 180°C for 12h and then cooled to room temperature to give a white product, which was collected by filtration, washed with hot DMF and acetone, and dried in the air. Yield: 300 mg [$[Ti_2(O)_2(C_{16}H_6O_8)(H_2O)_2(C_3H_6O)_{0.7}]$] (60%) (average of five parallel reactions). The synthesis can be readily scaled up or down using the same ratio of reactants. Analytically calculated (Found) for $[Ti_2(O)_2(C_{16}H_6O_8)(H_2O)_2(C_3H_6O)_{0.7}]$ %: Ti 18.0, (18.1); C 41.0 (41.2); H 2.70 (2.36); N 0.0 (0.0).

Adsorption isotherms and cycling experiments

In a typical gas adsorption experiment, ca. 50 mg of MFM-300(Ti) was loaded into the IGA system and activated at 333K for 2 h and then heated to 423 K under dynamic high vacuum (1×10^{-8} mbar) for 12 h to give fully desolvated MFM-300(Ti) for the isotherm experiment.

Gravimetric sorption isotherms (0-1.0 bar) for NH_3 were recorded at different temperatures, maintained using a temperature-programmed water bath, on a Hiden Isochema IGA-003 system under ultra-high vacuum (10^{-10} bar) using a turbo pumping system. Research-grade NH_3 was purchased from BOC and used as received. For cycling experiments, trace amounts of water in the NH_3 were removed, and the pressure of NH_3 was increased from vacuum (1×10^{-8} mbar) to 100 mbar and the uptake recorded. The pressure was reduced to regenerate the sample with no assisted heating. This cycling process was repeated multiple times.

Volumetric cryogenic CO_2, isotherms were performed on Tristar II Plus using ultrahigh purity CO_2 at 195 K for void volumetric determination. The BET surface area was calculated using the software integrated into the instrument.

Breakthrough experiment

The MOF sample was activated at 393 K under dynamic vacuum for 16 h before breakthrough experiments, and 100 mg of desolvated sample packed into fixed-bed reactors. The sample was heated to 423 K under He flow for 2 h to achieve further activation. The fixed-bed was cooled to 298 K and the breakthrough experiment performed with a stream of 1000 ppm NH_3 diluted in He. The flow rate of the gas mixture was 100 mL min^{-1}. A Bruker Matrix MG5 FTIR spectrometer was used to analyze the outlet gases for detection of NH_3. The gas concentration, C, of NH_3 at the outlet was compared with the corresponding inlet concentration C_0, where $C/C_0 = 1$ indicates complete breakthrough. To determine the dynamic adsorption capacity, the uptake of each component (n_m) was calculated based on the breakthrough curves by the following equation:

$$V_m = -\frac{\int_0^t v_{gas\ out} dt - V_{dead}}{W_{MOF}} \quad [1]$$

$$n_m = \frac{PV_m}{RT} \quad [2]$$

where $V_{gas\ out}$ is the flow rate of the target gas with the unit of mL min^{-1}, V_{dead} is the dead volume of the system (mL), W represents the mass of sample packed in the breakthrough bed (g), t is the retention time for the specific gas (min), P is pressure (kpa), R is gas constant, and T is the measurement temperature (K).

Elemental Analysis

Elemental analysis for C, H and N content of complexes was carried out using a CE-440 Elemental Analyser manufactured by Exeter Analytical. Element analysis for Ti was carried out using ICP-OES measurements on a Perkin-Elmer Optima 2000.

Thermogravimetric analysis (TGA) Measurements

Thermogravimetric analysis was carried out under a flow of air (5 mL min^{-1}) with a heating rate of 5 °C min^{-1} on a Perkin-Elmer Pyris1 Thermogravimetric analyser. TGA data for MFM-300(Ti) is shown in Figure S3.

Fitting of isotherm data to the dual-site Langmuir-Freundlich model.

Adsorption isotherms of NH_3 in MFM-300(Ti) were fitted using the dual-site Langmuir-Freundlich model [Equation 3], where n is the amount adsorbed in in mmol g^{-1}, P is the pressure in bar, q_{sat} is the saturation capacity in mmol g^{-1} , b_1 is the Langmuir parameter in bar^{-1} , and v_1 and v_2 are the Freundlich parameters for two sites 1 and 2. All values of R^2 for the fits are > 0.98 confirming an excellent fit to the model. Fittings for MFM-300(Ti) are shown in Figure S7

$$n = \frac{q_{sat1} b_1 P^{v_1}}{1 + b_1 P^{v_1}} + \frac{q_{sat2} b_2 P^{v_2}}{1 + b_2 P^{v_2}} \qquad [3]$$

Analysis and derivation of the isosteric heat of adsorption for adsorption of NH_3 for MFM-300(Ti)

Isotherms at 273-308 K were used to estimate the isosteric enthalpies (ΔH) for NH_3 in MFM-300(Ti) and were fitted to the van 't Hoff equation [4];

$$lnP = -\frac{\Delta H}{RT} + \frac{\Delta S}{R} \qquad [4]$$

where P is pressure in bar, T is the temperature in K, and R is the ideal gas constant. All linear fittings show R^2 above 0.98 confirming the consistency of the isotherm data and of the fitting. These results are summarized in Table S1 for MFM-300(Ti).

Neutron Powder Diffraction (NPD)

Structural determination of the binding positions of ND_3 within MFM-300(Ti) were conducted on WISH, a long-wavelength powder and single-crystal neutron diffractometer at the ISIS neutron and muon facility at Rutherford Appleton Laboratory (UK). The instrument incorporates a solid methane moderator, providing a high flux of cold neutrons with a large bandwidth, which is transported to the sample *via* an elliptical guide. The divergence jaws of WISH allow tuning of the resolution according to the need of the experiment; in this case, it was setup in high-resolution mode. The WISH detectors are 1 m long, 8 mm diameter pixelated 3He tubes positioned at 2.2 m from the sample and arranged on a cylindrical locus covering a 2θ scattering angle of 10–170°. To reduce the background from the sample environment, WISH is equipped with an oscillating radial collimator that defines a cylinder of radius of approximately 22 mm diameter at 90° scattering. The sample of desolvated MFM-300(Ti) was loaded into a cylindrical vanadium sample container with an indium vacuum seal connected to a gas handling system. The sample was degassed at 1×10^{-7} mbar and at 383 K for 4 days with He flushing to remove any remaining trace guest water molecules. The sample was dosed with ND_3 using the volumetric method at room temperature to ensure that the gas was well dispersed throughout the crystalline structure of MFM-300(Ti). Data collection was performed at 10 ± 0.2 K, controlled using a helium cryostat.

Synchrotron Fourier Transform Infrared (FTIR) microspectroscopy

In situ gas-loaded synchrotron FTIR microspectroscopy was carried out at the Multimode InfraRed Imaging and Microspectroscopy (MIRIAM) beamline at the Diamond Light Source, Harwell Science Campus (UK). The instrument is comprised of a Bruker Hyperion 3000 microscope in transmission mode with a 15× objective and liquid-N_2-cooled MCT detector, coupled to a Bruker Vertex 80V FTIR interferometer using radiation generated from a bending magnet source. Spectra were collected (512 scans) in the range 500–4000 cm^{-1} at 4 cm^{-1} resolution and infrared spot size at the sample of approximately 15 × 15 μm. Samples were placed onto a zinc selenide (ZnSe) disk and placed within a Linkam FTIR 600 gastight sample cell, which was equipped with ZnSe windows, a heating stage, and gas inlet and outlets. The N_2 (Air products, high purity BIP grade) was used as supplied.

NH_3 was dosed volumetrically into the sample cell using mass flow controllers, the total flow rate being maintained at 100 cm^3 min^{-1} for all experiments. The gases were directly vented to an exhaust system, and the total pressure in the cell was maintained at 1 bar for all experiments. The sample was desolvated under a flow of dry N_2 at 100 cm^3 min^{-1} and 423 K for 3 h, and then cooled to room temperature under a continuous flow of N_2.

Inelastic neutron scattering

INS spectra were collected on the TOSCA beamline at ISIS Neutron and Muon Source (UK). The sample of desolvated MFM-300(Ti) was loaded into a cylindrical vanadium sample container with an indium vacuum seal and this was connected to a gas handling system. The sample was degassed at 393 K and 10^{-7} mbar for 24 h to remove any residual trace of guest water. The temperature during data collection was controlled using a closed cycle refrigerator cryostat (10 ± 0.1 K). The loading of NH_3 was performed volumetrically at room temperature, and subsequently the temperature was reduced to 10 K in order to minimize achievable thermal motion of the framework and adsorbed NH_3 molecules in the scattering measurements. Background spectra of MFM-300(Ti) were subtracted to obtain the difference spectra.

Modelling by Density Functional Theory (DFT) of the bare and NH_3-loaded MFM-300(Ti) was performed using the Vienna Ab initio Simulation Package (VASP)[2]. The calculation used the Projector Augmented Wave (PAW) method[3,4] to describe the effects of core electrons, and Perdew-Burke-Ernzerhof (PBE)[5] implementation of the Generalized Gradient Approximation (GGA) for the exchange-correlation functional. The energy cutoff was 800 eV for the plane-wave basis of the valence electrons. The lattice parameters and atomic coordinates determined by neutron powder diffraction in this work were used as the initial structure, and the electronic structure was calculated on the Γ-point for the unit cell (144 atoms for the blank MOF). The total energy tolerance for electronic energy minimization was 10^{-8} eV, and for structure optimization it was 10^{-7} eV. The maximum interatomic force after relaxation was below 0.001 eV/Å, and the optB86b-vdW functional for dispersion corrections was applied.[6] The vibrational eigen-frequencies and modes were calculated by solving the force constants and dynamical matrix using Phonopy.[7] The OClimax software was used to convert the DFT-calculated phonon results to the simulated INS spectra.[8]

Figures and Tables

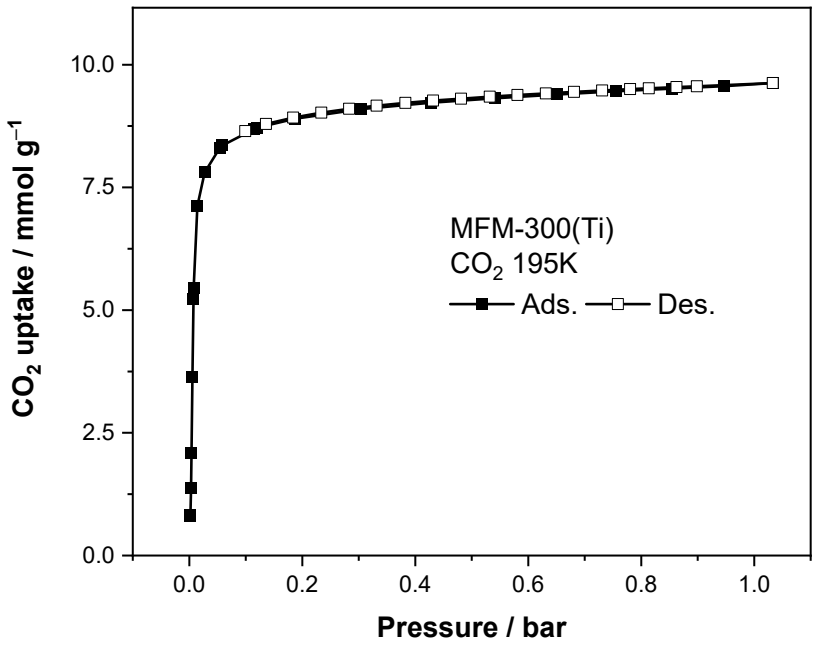

Figure S1. CO_2 adsorption data for MFM-300(Ti) at 195 K.

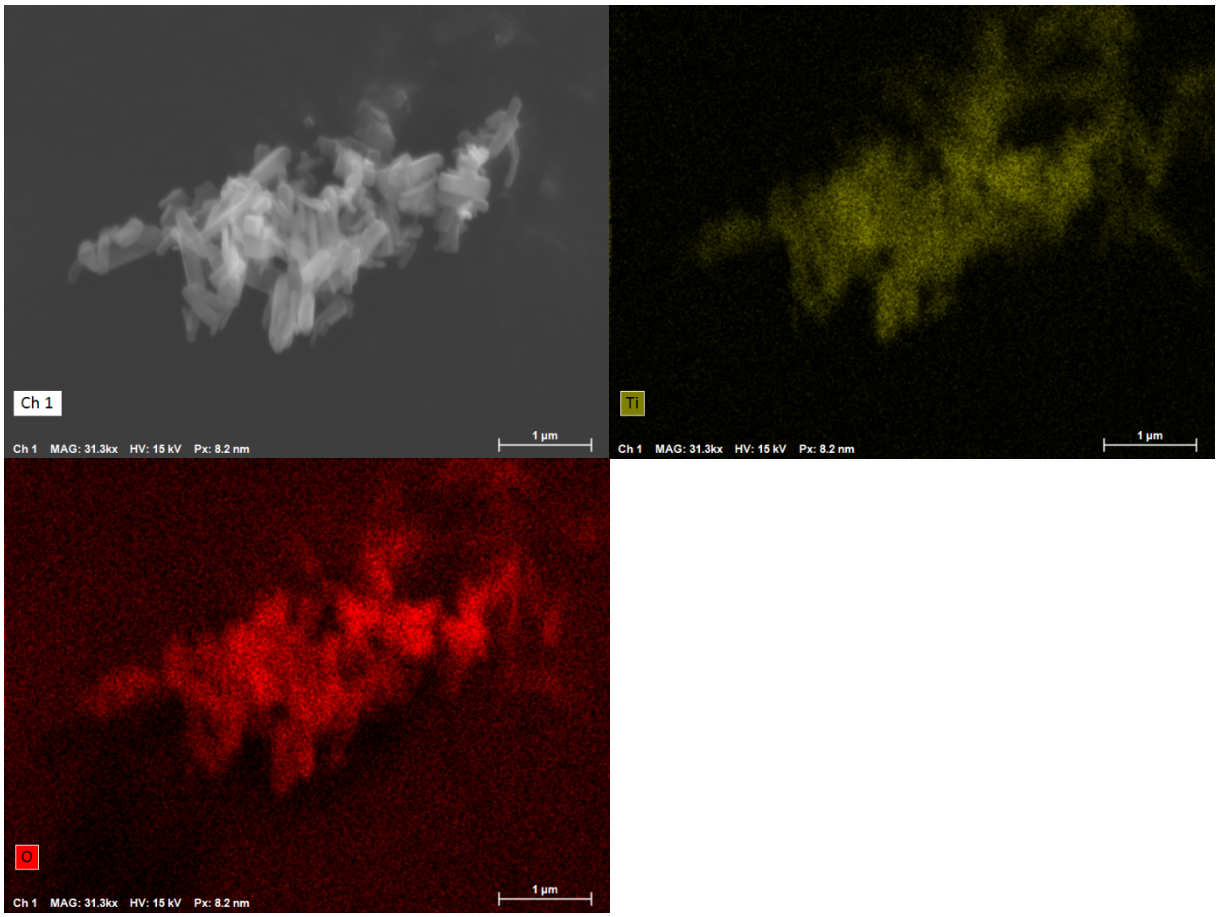

Figure S2. SEM and EDX images of MFM-300(Ti)**.**

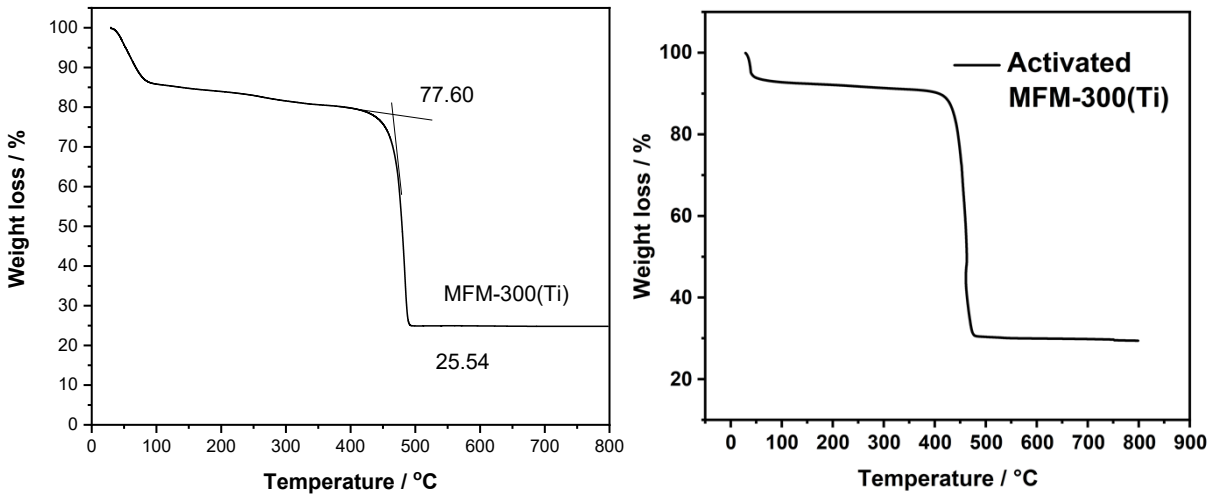

Figure S3. TGA plots for as-synthesised (a) and desolvated (b) MFM-300(Ti) at a heating rate of 5 °C min^{-1} from 40 °C to 800 °C in air. In figure a, the weight loss below 150 °C corresponds to the free solvents in the pore. The weight loss between 400 and 500 °C corresponds to the decomposition of the organic ligand, and the residue is titanium oxide. In figure b, the minor weight loss below 100 °C is likely due to the surface water adsorbed during the sample transfer.

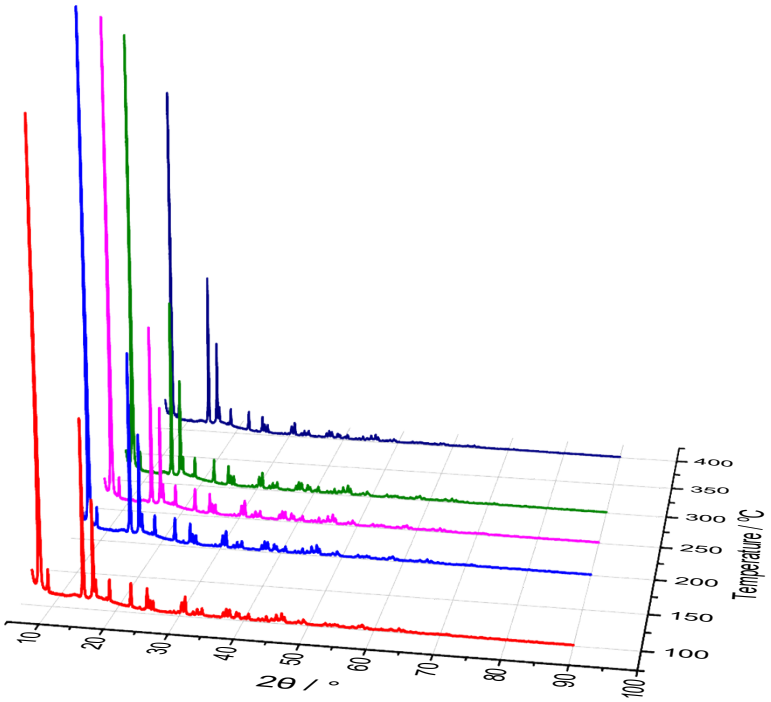

Figure S4. PXRD patterns of MFM-300(Ti) at different temperatures.

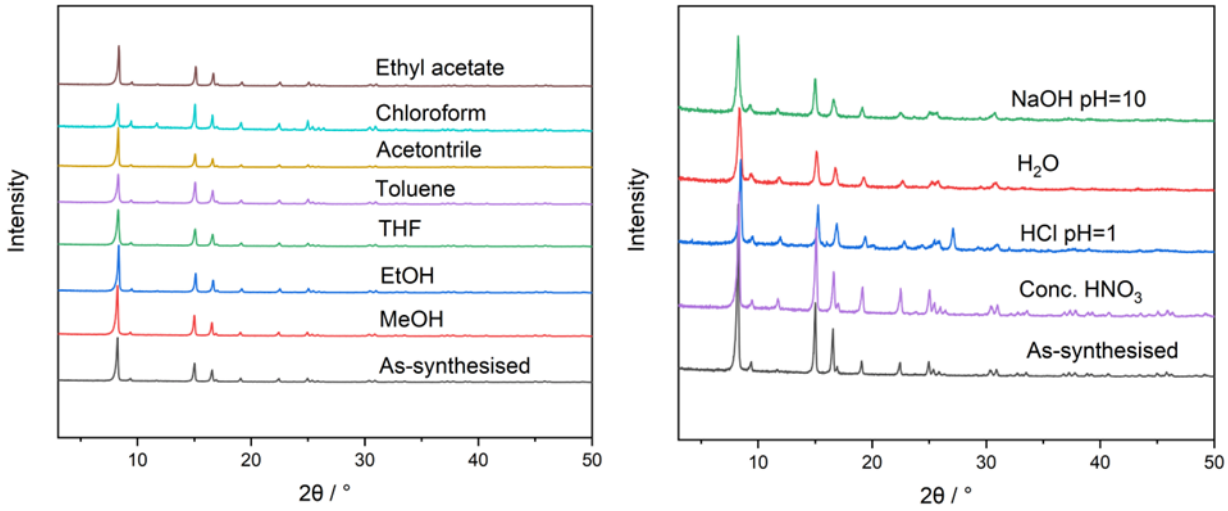

Figure S5. PXRD patterns of MFM-300(Ti) under different conditions.

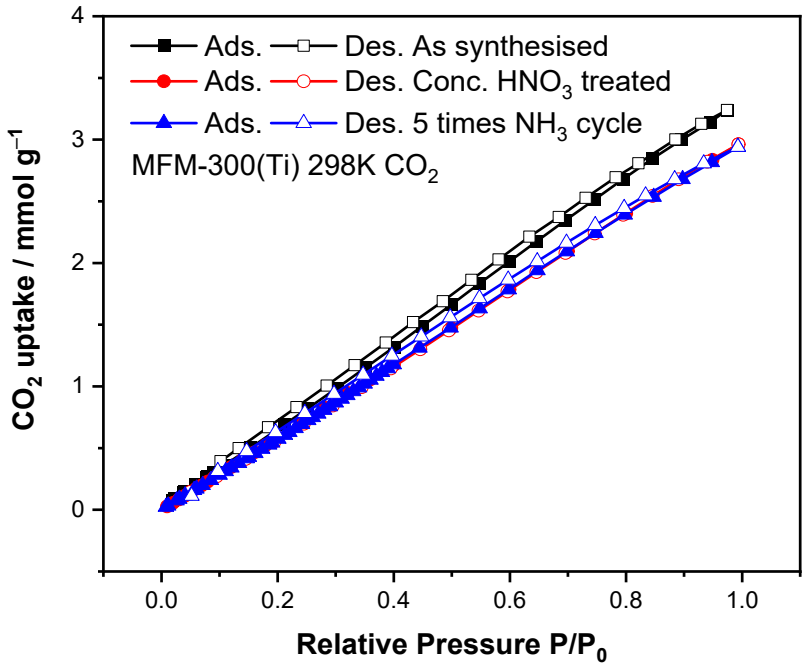

Figure S6. CO_2 adsorption data of activated, concentrated HNO_3 treated, and post NH_3-ads-des MFM-300(Ti) at 298 K.

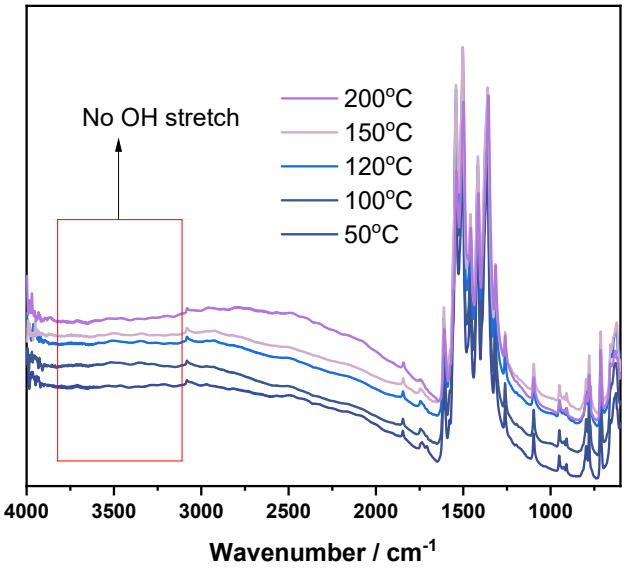

Figure S7. *In situ* synchrotron FTIR spectra of MFM-300(Ti) as a function of temperature under a dry N_2 flow at 100 mL min^{-1}.

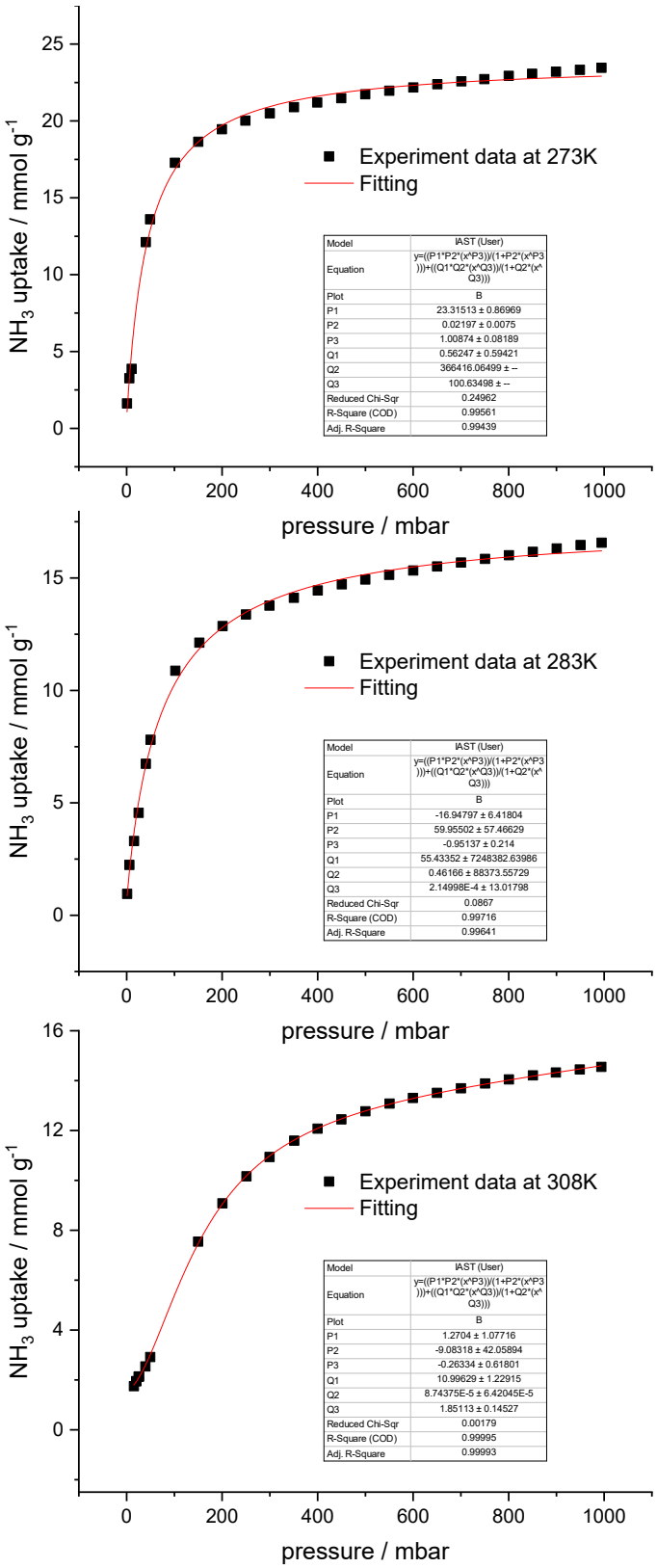

Figure S8. Fitting of isotherm data to the Dual-Site Langmuir-Freundlich Model.

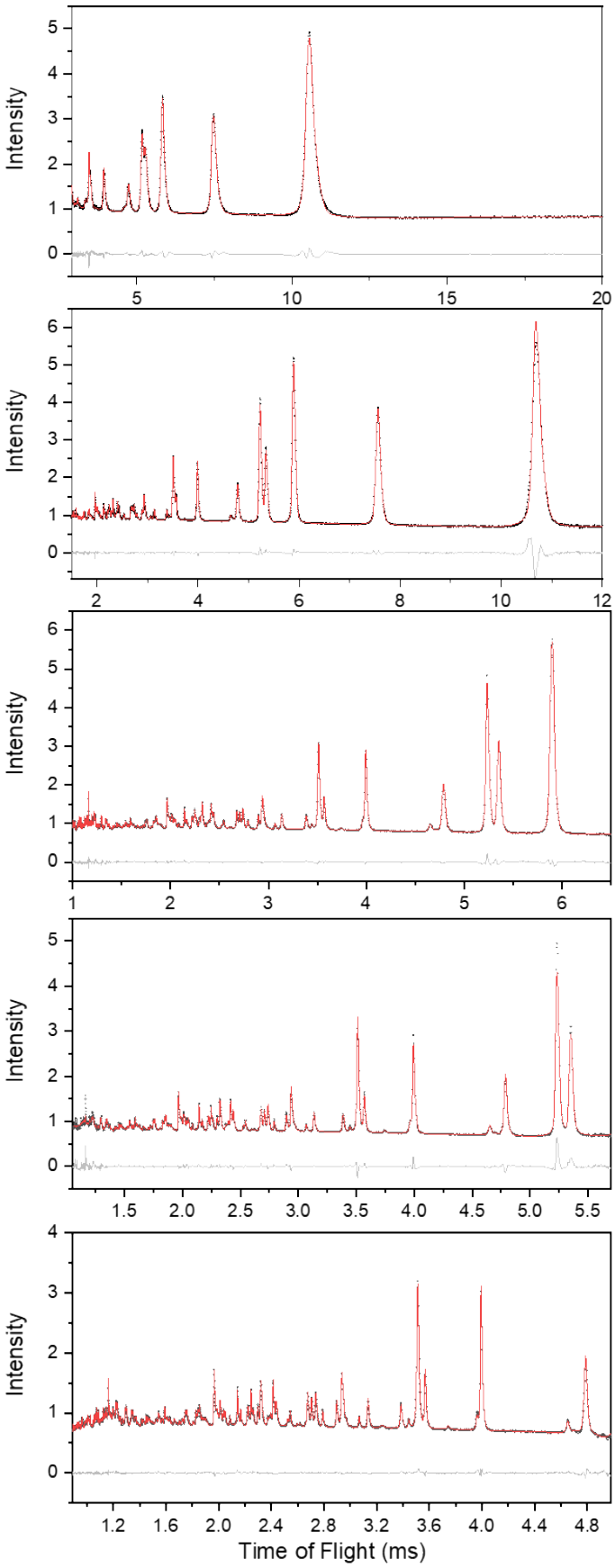

Figure S9. Neutron diffraction patterns and Rietveld refinement for MFM-300(Ti) (banks 1 to 5 from top to bottom).

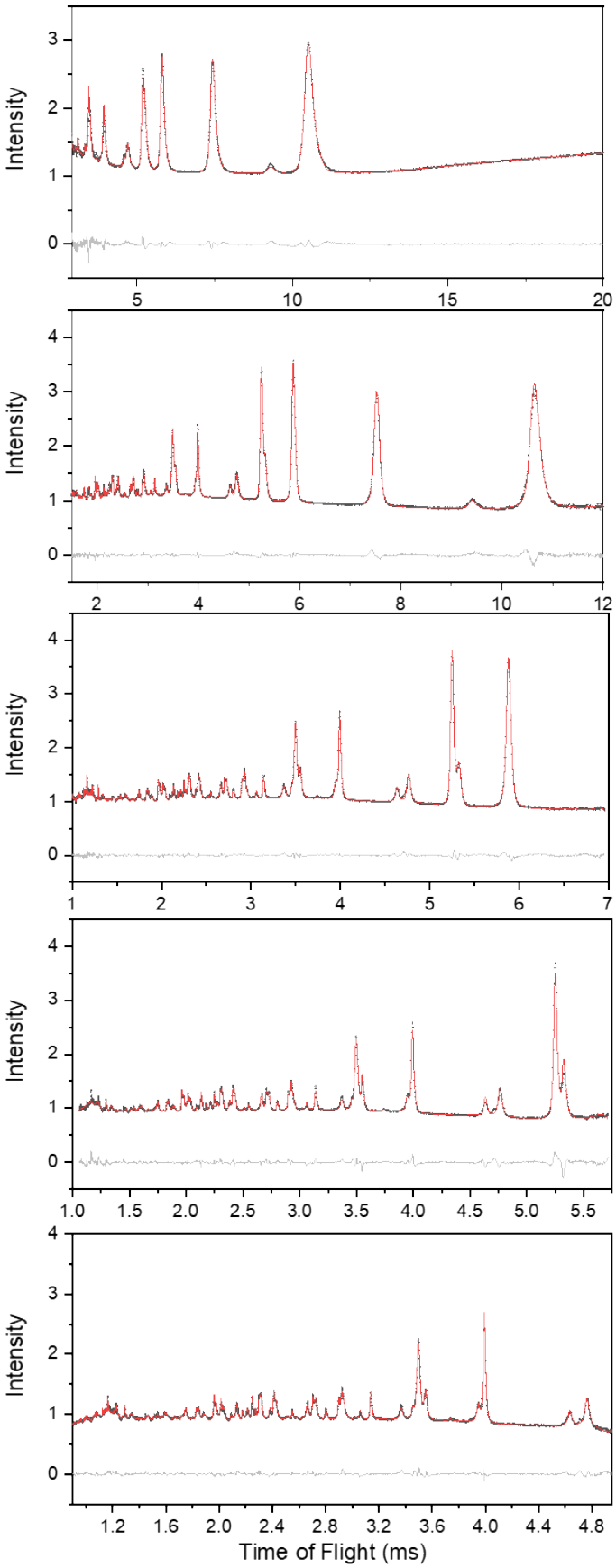

Figure S10. Neutron diffraction patterns and Rietveld refinement for MFM-300(Ti)·0.84 ND_3 (banks 1 to 5 from top to bottom).

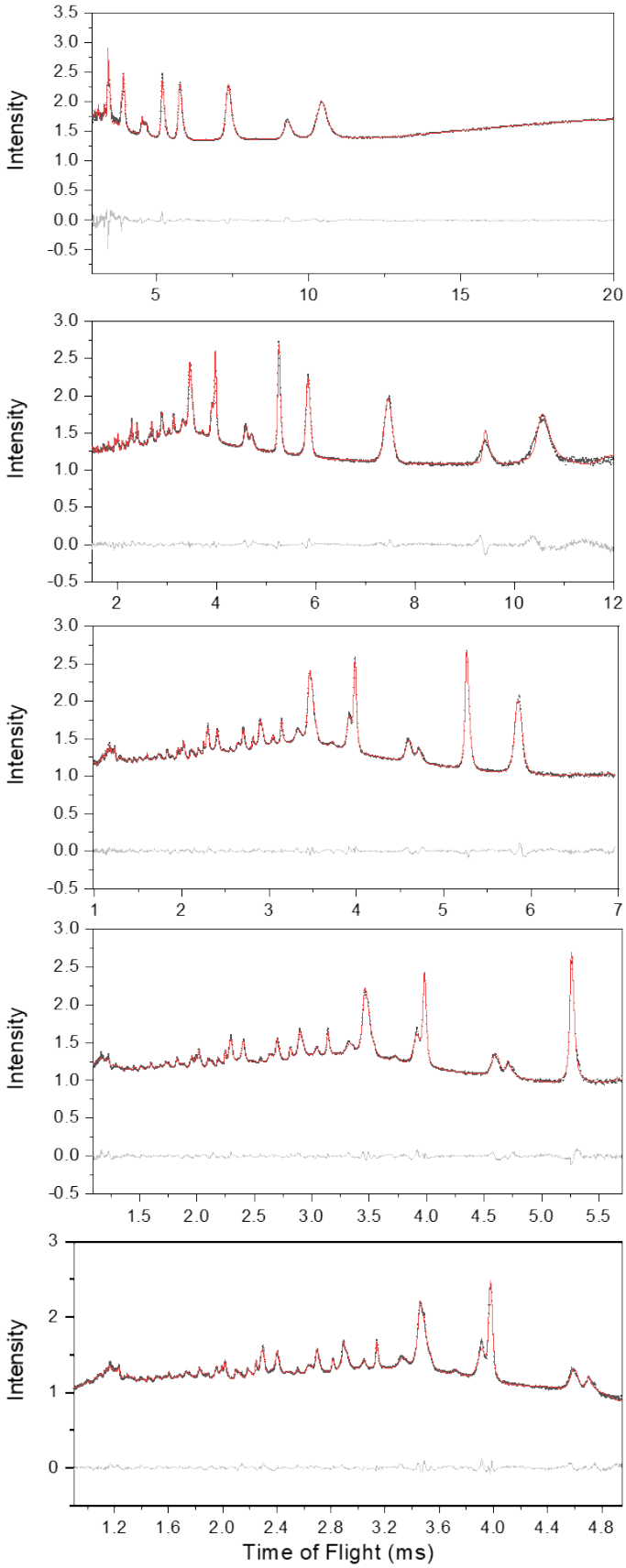

Figure S11. Neutron diffraction patterns and Rietveld refinement for MFM-300(Ti)·2.54 ND_3 (banks 1 to 5 from top to bottom).

Inelastic neutron scattering

INS was applied to study the binding interaction and structure dynamics in this case because of its several unique advantages:

(a) INS spectroscopy is ultra-sensitive to the vibrations of hydrogen atoms, which is ten times more visible than other elements due to its high neutron cross-section.

(b) The technique is not subject to any optical selection rules, neither restricted to the centre of the Brillouin zone (gamma point). All vibrations are active and, in principle, measurable.

(c) INS spectra can be readily and accurately modelled: the intensities are proportional to the concentration of elements in the sample and their cross-sections, and the measured INS intensities relate straightforwardly to the associated displacements of the scattering atom. Treatment of background correction is also relatively straightforward.

(d) Neutrons penetrate deep into materials and pass readily through the walls of metal containers making neutrons ideal to measure bulk properties of materials.

(e) INS spectrometers cover the whole range of the molecular vibrational spectrum, 0–500 meV (0-4000 cm^{-1}).

(f) Calculation of the INS spectra by DFT vibrational analysis can be readily achieved, and DFT calculations relate directly to the INS spectra, and, in the case of solid-state calculations, there are no approximations other than the use of DFT eigenvectors and eigenvalues to determine the spectral intensities. Assignments of features on the experimental difference spectra are described in main text.

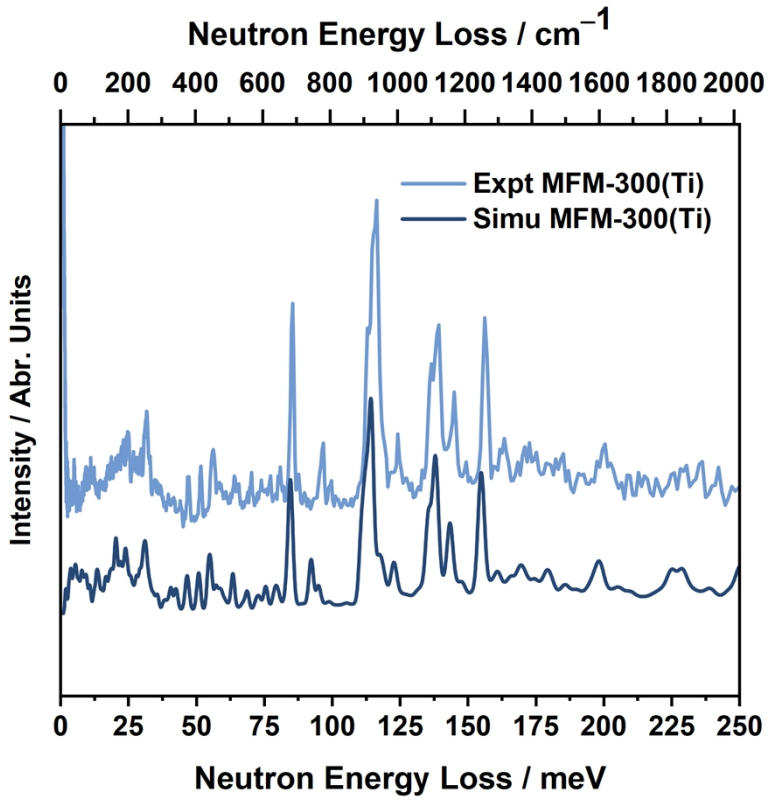

Figure S12. Experimental and simulated INS spectra of MFM-300(Ti).

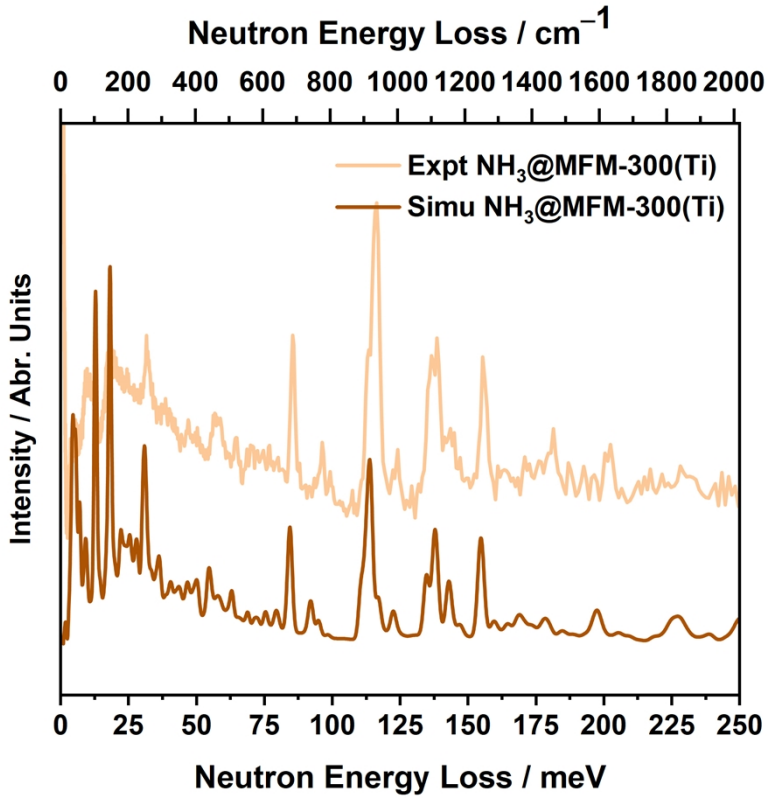

Figure S13. Experimental and simulated INS spectra of NH_3-loaded MFM-300(Ti).

Table S1. Summary of the pore volume, NH_3 isothermal adsorption capacities and NH_3 packing density in stable MOF materials.

MOF	Measuring condition	Pore volume ($cm^3\ g^{-1}$)	NH_3 isothermal uptake ($mmol\ g^{-1}$)	NH_3 packing density/g cm^{-3}	Reference
MFM-300(Ti)	**298 K 1.0 bar**	**0.47** [b]	**16.1**	**0.58**	**This work**
	273 K 1.0 bar		**23.4**	**0.84**	**This work**
43.4% LiCl@MIL-53-$(OH)_2$	298 K 1.0 bar	n/a	33.9	n/a	9
M_2(dobpdc) (M=Mn, Co, Ni, Mg)	298 K 1.0 bar	1.18, 1.06, 1.11, 1.60[a]	13.3, 13.3, 20.8, 23.9	0.19, 0.21, 0.32, 0.25	10
Ni_acryl_TMA	298 K 1.0 bar	0.57[a]	23.5	0.70	11
Ni_acryl_TGA	298 K 1.0 bar	0.56[a]	17.4	0.53	11
MOF-303	298 K 1.0 bar	0.55[a]	19.7	0.61 (293 K)	12
MFM-300(M) (M=V^{III}, V^{IV}, Fe)	273 K 1.0 bar	0.49, 0.48, 0.46[a]	16.1, 17.3, 15.6	0.54, 0.61, 0.60	13
UiO-66-X (M=defect, Cu^{I}, Cu^{II})	273 K 1.0 bar	0.388[b]	11.8, 12.6, 16.9	0.52, 0.55, 0.74	14
MFM-300(Al)	273 K 1.0 bar	0.37[c]	15.7	0.72	15
M_2Cl_2BTDD (M=Mn, Co, Ni)	298 K 1.0 bar	n/a	15.5, 12.0, 12.0	n/a	16
MFM-300(Sc)	298 K 1.0 bar	0.48[a]	13.1	0.46	17
MIL-160	298 K 1.0 bar	0.45[a]	12.8	0.48	18
$M_2(adc)_2$(dabco) (M=Zn, Co, Ni)	295 K 1.0 bar	0.25[a]	8.3, 11.2, 12.1	0.56, 0.76, 0.82	19
MFM-303(Al)	293 K 1.0 bar	0.191[b]	9.0	0.80	20
NU-1401	298 K 1.0 bar	0.23[a]	8.4	0.62	21
Al-PMOF	298 K 1.0 bar	n/a	7.7	n/a	22

[a]: pore volume determined from N_2 isotherms at 77 K.

[b]: pore volume from crystal structure.

[c]: pore volume determined from CO_2 isotherms at 195 K.

Table S2. Thermodynamic parameters for NH_3 adsorption in MFM-300(Ti).

n mmol g^{-1}	Q_{st} kJ mol^{-1}	Q_{st} error kJ mol^{-1}	ΔS J K^{-1} mol^{-1}	ΔS error J K^{-1} mol^{-1}	R^2
3.0	43.8	3.42	-212	11.7	0.987
3.5	43.7	3.37	-214	11.6	0.988
4.0	43.3	3.40	-214	11.6	0.988
4.5	42.9	3.48	-213	11.9	0.987
5.0	42.4	3.58	-213	12.3	0.986
5.5	41.9	3.69	-212	12.6	0.985
6.0	41.5	3.80	-212	13.0	0.983
6.5	41.1	3.89	-211	13.3	0.982
7.0	40.8	3.95	-211	13.5	0.981
7.5	40.5	3.98	-211	13.7	0.981
8.0	40.3	3.97	-211	13.6	0.981
8.5	40.3	3.91	-212	13.4	0.981
9.0	40.3	3.78	-212	12.9	0.982
9.5	40.4	3.57	-214	12.2	0.985
10.0	40.7	3.26	-216	11.2	0.987
10.5	41.2	2.84	-218	9.74	0.991
11.0	41.9	2.30	-221	7.89	0.994
11.5	42.8	1.64	-226	5.60	0.997
12.0	44.1	0.87	-231	2.98	0.999
12.5	45.7	0.07	-237	0.238	1.000
13.0	47.6	0.68	-245	2.33	0.999
13.5	49.8	1.32	-254	4.52	0.999
14.0	52.2	1.90	-264	6.51	0.997
14.5	54.4	2.58	-273	8.86	0.995

Table S3. Crystallography data for MFM-300(Ti).

Sample Name	MFM-300(Ti)-desolvated	MFM-300(Ti)·0.84ND_3	MFM-300(Ti)·2.54ND_3
CCDC number	2296493	2296494	2296495
Crystal system	Tetragonal	Tetragonal	Tetragonal
Space Group	I 4_1 2 2	I 4_1 2 2	I 4_1 2 2
Formula	$[Ti_2(O)_2bptc]$	$[Ti_2(O)_2bptc]$ $(ND_3)_{0.84}$	$[Ti_2(O)_2bptc]$ $(ND_3)_{2.54}$
a (Å)	15.1203(4)	15.0507(8)	14.9200(4)
b (Å)	15.1203(4)	15.0507(8)	14.9200(4)
c (Å)	11.9863(3)	12.0595(6)	12.1536(3)
beta (°)	90	90	90
Cell Volume /Å^3	2740.33(17)	2731.8(3)	2705.47(15)
Cell density g/cm^3	1.100	1.138	1.221
Method	Rietveld	Rietveld	Rietveld
Radiation	Neutron	Neutron	Neutron
Scan method	Time of flight	Time of flight	Time of flight
R_{wp} (%)	1.843	1.600	1.206
R_{exp}(%)	0.514	0.483	0.430
GOF	3.581	3.312	2.808

Table S4. Atomic positions for atoms in MFM-300(Ti).

	X	y	z	Occupancy	Biso / Å2
Ti	0.6968(2)	0.3032(2)	0.5	1	1.60(16)
O1	0.74212(17)	0.25	0.625	1	0.98(5)
O2	0.6178(3)	0.3765(3)	0.6064(2)	1	0.98(5)
O3	0.6032(3)	0.2890(2)	0.7571(3)	1	0.98(5)
C1	0.5903(2)	0.36112(17)	0.70484(18)	1	1.15(3)
C2	0.54079(7)	0.43068(6)	0.76148(15)	1	1.15(3)
C3	0.5	0.5	0.70290(18)	1	1.15(3)
C4	0.54079(7)	0.43068(6)	0.87864(10)	1	1.15(3)
C5	0.5	0.5	0.93722(9)	1	1.15(3)
H3	0.5	0.5	0.6153(3)	1	1.38(4)
H4	0.57129(14)	0.37884(17)	0.92244(16)	1	1.38(4)

Table S5. Host-guest interactions in MFM-300(Ti)·$(ND_3)_{0.84}$

MFM-300(Ti))·$(ND_3)_{0.84}$	Interactions	Distance (Å)	Colour
Site I	$ND_3\cdots O_{ligand}$	2.10(2)	Yellow
	$ND_3\cdots O_{ligand}$	2.25(3)	Yellow
	$ND_3\cdots O_{ligand}$	2.97(3)	Yellow
Site II	$ND_3\cdots O_{ligand}$	2.99(8)	Yellow
	$ND_3\cdots$aromatic rings	2.73(15)	Green

Table S6: Atomic positions in MFM-300(Ti)·$(ND_3)_{0.84}$.

	x	Y	Z	Occupancy	Biso / Å^2
Ti	0.6951(3)	0.3049(3)	0.5	1	0.5(2)
O1	0.7332(3)	0.25	0.625	1	1.36(8)
O2	0.6171(5)	0.3786(5)	0.6084(4)	1	1.36(8)
O3	0.6006(5)	0.2885(4)	0.7634(5)	1	1.36(8)
C1	0.5916(3)	0.3583(3)	0.7054(3)	1	2.04(6)
C2	0.54100(12)	0.43063(10)	0.7626(2)	1	2.04(6)
C3	0.5	0.5	0.7045(3)	1	2.04(6)
C4	0.54100(12)	0.43063(10)	0.87869(17)	1	2.04(6)
C5	0.5	0.5	0.93675(16)	1	2.04(6)
H3	0.5	0.5	0.6208(6)	1	2.45(7)
H4	0.5705(3)	0.3806(3)	0.9205(3)	1	2.45(7)
N_1_2	0.5792(13)	0.7071(8)	0.2201(18)	0.0716(19)	1.0(7)
D_2_2	0.521(6)	0.675(10)	0.234(3)	0.0716(19)	1.2(8)
D_3_2	0.593(2)	0.699(4)	0.1381(19)	0.0716(19)	1.2(8)
D_4_2	0.626(7)	0.672(8)	0.262(3)	0.0716(19)	1.2(8)
N_1_1	0.5546(9)	0.6910(8)	0.4351(12)	0.137(2)	10.0(8)
D_2_1	0.545(2)	0.707(2)	0.5164(14)	0.137(2)	12.0(10)
D_3_1	0.4935(13)	0.696(2)	0.399(3)	0.137(2)	12.0(10)
D_4_1	0.570(2)	0.6250(10)	0.434(3)	0.137(2)	12.0(10)

MFM-300(Ti))·$(ND_3)_{2.54}$		Interactions	Distance (Å)		Colour
Site I		$ND_3\cdots O_{ligand}$	2.14(3)		Yellow
	x	$ND_3\cdots$Oligand	z2.55(3)	Occupancy	Yellow Biso / Å^2
Site II		$ND_3\cdots$aromatic rings	2.52(3)		Green
Ti	0.6858(6)	0.3142(6)	0.5	1	0.5(4)
O1	0.7266(5)	0.25	0.625	1	0.50(9)
Site III		$ND_3\cdots O_{bridge}$	2.47(6)		Yellow
		$ND_3\cdots O_{ligand}$	1.92(5)		Yellow
		$ND_3\cdots O_{ligand}$	2.33(6)		Yellow
		$ND_3\cdots O_{ligand}$	2.38(6)		Yellow
		$ND_3\cdots O_{ligand}$	2.78(6)		Yellow
		$D_3N\cdots H–C_{aromatic}$	1.50(3)		Light blue
		$D_3N\cdots H–C_{aromatic}$	2.24(3)		Light blue

Table S7: Host-guest interactions in MFM-300(Ti)·$(ND_3)_{2.54}$.

O2	0.6193(11)	0.3745(12)	0.6109(7)	1	0.50(9)
O3	0.5983(12)	0.2831(7)	0.7685(9)	1	0.50(9)
C1	0.5914(9)	0.3548(7)	0.7089(5)	1	3.25(8)
C2	0.5414(3)	0.4295(2)	0.7642(4)	1	3.25(8)
C3	0.5	0.5	0.7062(5)	1	3.25(8)
C4	0.5414(3)	0.4295(2)	0.8800(3)	1	3.25(8)
C5	0.5	0.5	0.9380(3)	1	3.25(8)
H3	0.5	0.5	0.6219(8)	1	3.90(10)
H4	0.5715(6)	0.3782(5)	0.9222(4)	1	3.90(10)
N_1_2	0.4232(7)	0.1894(7)	0.7852(6)	0.378(4)	10.0(5)
D_2_2	0.3770(14)	0.1988(19)	0.8459(15)	0.378(4)	12.0(6)
D_3_2	0.4270(17)	0.1218(8)	0.774(2)	0.378(4)	12.0(6)
D_4_2	0.4832(11)	0.2077(17)	0.818(2)	0.378(4)	12.0(6)
N_1_1	0.6905(8)	0.6090(7)	0.7488(11)	0.183(2)	1.0(4)
D_2_1	0.653(3)	0.5527(17)	0.762(2)	0.183(2)	1.2(5)
D_3_1	0.7338(14)	0.593(2)	0.6869(18)	0.183(2)	1.2(5)
D_4_1	0.7291(15)	0.617(3)	0.8173(16)	0.183(2)	1.2(5)
N_1_3	0.2993(18)	0.5827(18)	0.002(2)	0.075(2)	1.0(10)
H_2_3	0.267(4)	0.595(4)	0.075(4)	0.075(2)	1.2(12)
H_3_3	0.298(4)	0.642(3)	-0.040(5)	0.075(2)	1.2(12)
H_4_3	0.259(4)	0.540(4)	-0.040(5)	0.075(2)	1.2(12)

Table S8: Atomic positions in MFM-300(Ti)·$(ND_3)_{2.54}$·

Table S9: C-C bond length in MFM-300(Ti), MFM-300(Ti)·$(ND_3)_{0.84}$, and MFM-300(Ti)·$(ND_3)_{2.54}$.

Sample name	Bond type	Bond length
MFM-300(Ti)	C-C aromatic	1.458(2)
MFM-300(Ti)·$(ND_3)_{0.84}$		1.497(4)
MFM-300(Ti)·$(ND_3)_{2.54}$		1.500(7)

Author Contribution Section

XZ, JL and LG: synthesis and characterisation of materials, measurements of adsorption data. XZ, MH, WL, DC, YM, PM and SR: measurements and analysis of NPD and INS data, structure determination. XZ, MKJ and MDF: measurements and analysis of the FTIR data. MS and SY: overall direction of the project. XZ, MS and SY: preparation of the manuscript with contributions from all authors.

Supplementary References

1. S. Wang, H. Reinsch, N. Heymans, M. Wahiduzzaman, C. Martineau-Corcos, G. De Weireld, G. Maurin and C. Serre, *Matter*, 2020, **2**, 440-450.
2. G. Kresse and J. Furthmüller, *Phys. Rev. B*, 19d96, **54**, 11169.
3. P. E. Blöchl, *Phys. Rev. B*, 1994, **50**, 17953.
4. G. Kresse and D. Joubert, *Phys. Rev. B,* 1999, **59**, 1758.
5. J. P. Perdew, K. Burke and M. Ernzerhof, *Phys. Rev. Lett.*, 1996, **77**, 3865.
6. J. Klimeš, D. R. Bowler and A. Michaelides, *J. Phys.: Condens. Matter*, 2009, **22**, 022201.
7. A. Togo and I. Tanaka, *Scr. Mater.*, 2015, **108**, 1-5.
8. Y. Cheng, L. L. Daemen, A. I. Kolesnikov and A. J. Ramirez-Cuesta, *J. Chem. Theory Comput.*, 2019, **15**, 1974-1982.
9. Y. Shi, Z. Wang, Z. Li, H. Wang, D. Xiong, J. Qiu, X. Tian, G. Feng and J. Wang, *Angew. Chem. Int. Ed.,* 2022, **61**, e202212032.
10. D. W. Kim, D. W. Kang, M. Kang, J. H. Lee, J. H. Choe, Y. S. Chae, D. S. Choi, H. Yun and C. S. Hong, *Angew. Chem. Int. Ed.*, 2020, **59**, 22531-22536.
11. D. W. Kim, D. W. Kang, M. Kang, D. S. Choi, H. Yun, S. Y. Kim, S. M. Lee, J.-H. Lee and C. S. Hong, *J. Am. Chem. Soc.*, 2022, **144**, 9672-9683.
12. Z. Wang, Z. Li, X.-G. Zhang, Q. Xia, H. Wang, C. Wang, Y. Wang, H. He, Y. Zhao and J. Wang, *ACS Appl. Mater. Interfaces,* 2021, **13**, 56025-56034.
13. X. Han, W. Lu, Y. Chen, I. Da Silva, J. Li, L. Lin, W. Li, A. M. Sheveleva, H. G. Godfrey, Z. Lu, F. Tuna, E. J. L. McInnes, Y. Cheng, L. L. Daemen, L. J. M. McPherson, S. J. Teat, M. D. Frogley, S. Rudić, P. Manuel, A. J. Ramirez-Cuesta, S. Yang and M.Schröder, *J. Am. Chem. Soc.*, 2021, **143**, 3153-3161.
14. Y. Ma, W. Lu, X. Han, Y. Chen, I. Da Silva, D. Lee, A. M. Sheveleva, Z. Wang, J. Li and W. Li, M. Fan, S. Xu, F. Tuna, E. J. L. McInnes, Y. Cheng, , S. Rudić, P. Manuel, M. D. Frogley, A. J. Ramirez-Cuesta, M.Schröder and S. Yang, *J. Am. Chem. Soc.*, 2022, **144**, 8624-8632.
15. H. G. Godfrey, I. da Silva, L. Briggs, J. H. Carter, C. G. Morris, M. Savage, T. L. Easun, P. Manuel, C. A. Murray, C. C. Tang, M. D. Frogley, G. Cinque, S. Yang and M.Schröder, *Angew. Chem. Int. Ed.*, 2018, **130**, 14994-14997.
16. A. J. Rieth, Y. Tulchinsky and M. Dincă, *J. Am. Chem. Soc.*, 2016, **138**, 9401-9404.
17. L. Guo, X. Han, Y. Ma, J. Li, W. Lu, W. Li, D. Lee, I. Da Silva, Y. Cheng, S. Rudić, P. Manuel, M. D. Frogley, A. J. Ramirez-Cuesta, M.Schröder and S. Yang, *Chem. Commun.*, 2022, **58**, 5753-5756.
18. L. Guo, J. Hurd, M. He, W. Lu, J. Li, D. Crawshaw, M. Fan, S. Sapchenko, Y. Chen, X. Zeng, M. Kippax-Jones, W. Huang, Z. Zhu, P. Manuel, M. D. Frogley, D. Lee, M.Schröder and S. Yang, *Commun. Chem.,* 2023, **6**, 55.
19. Z. Cao, K. N. Landström and F. Akhtar, *Catalysts*, 2020, **10**, 1444.
20. C. Marsh, X. Han, J. Li, Z. Lu, S. P. Argent, I. Da Silva, Y. Cheng, L. L. Daemen, A. J. Ramirez-Cuesta S. P. Thompson, A. J. Blake, S. Yang and M.Schröder, *J. Am. Chem. Soc.*, 2021, **143**, 6586-6592.
21. Y. Zhang, X. Zhang, Z. Chen, K. i. Otake, G. W. Peterson, Y. Chen, X. Wang, L. R. Redfern, S. Goswami, P. Li, T. Islamoglu, B. Wang and O. K. Farha, *ChemSusChem*, 2020, **13**, 1710-1714.
22. J. Liu, Z. Lu, Z. Chen, M. Rimoldi, A. J. Howarth, H. Chen, S. Alayoglu, R. Q. Snurr, O. K. Farha and J. T. Hupp, *ACS Appl. Mater. Interfaces*, 2021, **13**, 20081-20093.